

A System for Digital Reconstruction of Gypsum Dental Casts

A. Ardeshir Goshtasby,* *Senior Member, IEEE*, Surya Nambala, Waldemar G. deRijk, and Stephen D. Campbell

Abstract—A range scanner is developed that can scan a gypsum dental cast and reconstruct the cast digitally for display and storage purposes. The scanner is based on subtractive light and computes the range values using optical triangulation. A fiducial marker is introduced that, when attached to a dental cast at the time of image acquisition, makes it possible to integrate multiview range images of the cast without image registration. A method for calibrating the scanner is described and experimental results showing the accuracy of the scanner are presented.

Index Terms—Calibration, dental cast, image integration, optical triangulation, range image.

I. INTRODUCTION

DENTAL casts are widely used in dentistry to plan treatment and design prostheses. To carry out three-dimensional (3-D) measures on a cast, stereo photogrammetry has been used [1]–[4]. Although the instrument used in stereo photogrammetry is simple, the user must interact with the instrument considerably to determine the 3-D coordinates of points on a cast.

Van der Linden *et al.* [5] designed a system called Optocom that could measure coordinates of 3-D points on a cast by a mechanical contact. Although this system produces accurate measurements, it is very labor intensive. A system known as Reflex Metrograph [6], [7] uses a noncontacting principle to measure the coordinates of 3-D points on a cast by aligning a movable light with a desired point on a cast behind a semireflecting mirror. Based on a similar principle, Traveling Microscope [8] was developed, which can measure 3-D coordinates on a cast without mechanical contacts. Measurements using the Reflex Metrograph and Traveling Microscope require less effort than do measurements using Optocom; however, because the measurements are obtained point by point, determination of a large number of points for reconstruction of a cast is very time consuming. Laser range scanners can determine the coordinates of points on a cast without user interaction [9]–[11], and can be used to obtain

dense elevation maps of a dental cast. A laser range scanner developed by Yamamoto *et al.* [12], [13] can generate single-view depth maps of a cast for visualization and quantification.

A system developed by Duret *et al.* [14] combines holographic and moiré techniques to produce an array of 3-D points that represents a single-view image of a tooth. Images from different views are then interactively combined, and a rigid theoretical tooth is fitted to the points to reconstruct the tooth analytically. With this system, a dental practitioner can personalize the anatomy of a tooth. This system can design a custom crown for a particular tooth and subsequent milling for immediate fabrication of a restoration. Similar systems have been developed by Heymann [15], Brandestini and Mörmann [16], and Rekow [17]. A comprehensive review of such a CAD/CAM system has been provided by Rekow [18].

In this paper, we will describe the development of a system that can construct a 3-D digital model of a dental cast by integrating multiview range images from the cast and fitting an elastic surface to the combined data. We introduce a special fiducial marker that, when attached to a dental cast at the time of scanning, makes it possible to integrate multiview images of the cast without image registration.

II. SCANNER CHARACTERISTICS

The organization of the scanner is shown in Fig. 1. White light is guided to the focal point of a lens through fiber optics (the white light source and fiber optics are from Edmund Scientific, Burrington, NJ, Models C-72 162 and C42,343). The point light source at the focal point of a lens with a focal length of 200 mm (symmetric-convex glass lens, Model 01LDX223, from Melles Griot, Irvine, CA) generates a cylindrical light toward a mirror. The mirror reflects the light on an object under a charge-coupled device (CCD) camera (Pulnix, Model TM-7AS, Sunnyvale, CA) that has a resolution of 512×512 pixels. Before reaching the object, the light is blocked by a thin fiber, creating a shadow profile on the object. We have used a strand of human hair as the fiber. Fig. 2 shows the kind of images obtained by this scanner. With the camera, the mirror, the object, the lens, and the light source fixed in their positions, a translation stage (Newport, Model UMR12.80, Irvine, CA) sweeps the hair over the object. The geometry of the shadow profiles are recorded by the camera and used to determine the coordinates of 3-D points on the object. The lens in front of the point light source is removable and can be replaced with other lenses to generate cylindrical directional lights of desired diameters. The camera's zoom and focal length can also be varied to scan objects of different

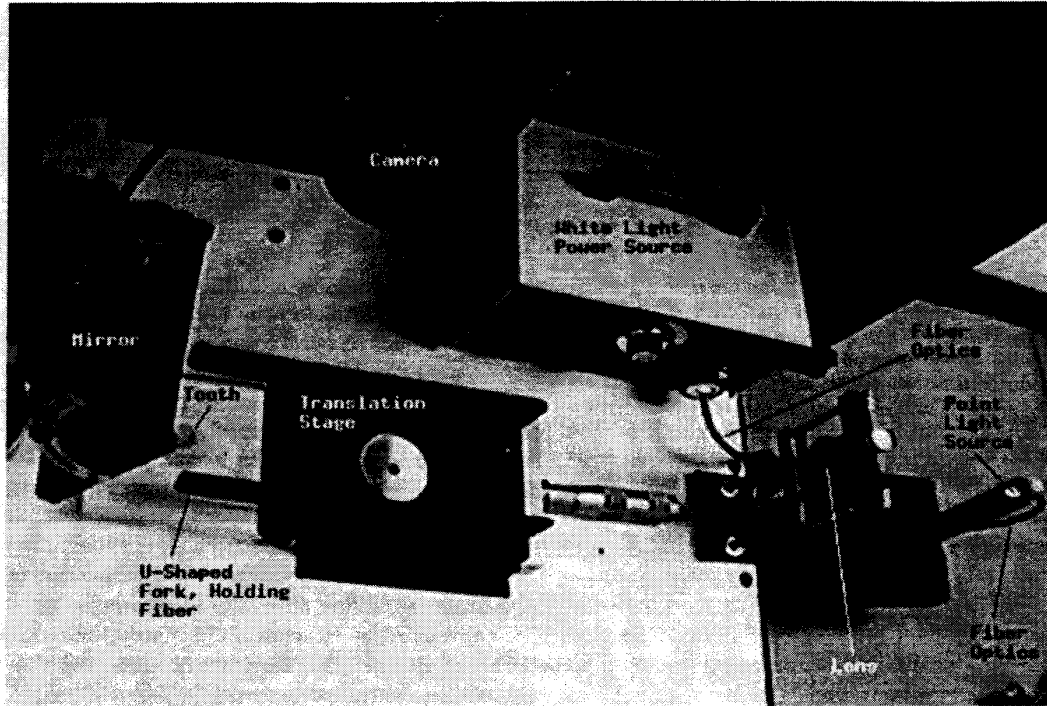
Manuscript received October 14, 1996; revised April 8, 1997. This work was supported in part by the National Institute of Dental Research under Grant IR03DE11162. The Associate Editor responsible for coordinating the review of this paper and recommending its publication was M. W. Vannier. *Asterisk indicates corresponding author.*

*A. A. Goshtasby is with the Computer Science and Engineering Department, Wright State University, 303 Russ Engineering Center, Dayton, OH 45435 USA (e-mail: agoshtas@cs.wright.edu).

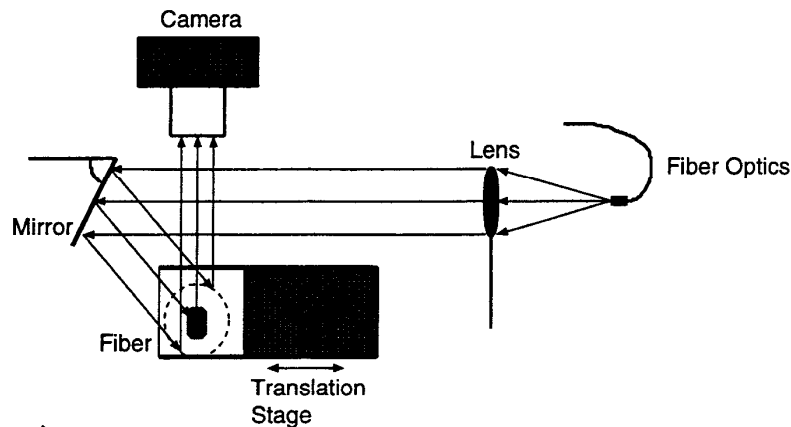
S. Nambala is with the Computer Science and Engineering Department, Wright State University, Dayton, OH 45435 USA.

W. G. deRijk and S. D. Campbell are with Restorative Dentistry, University of Illinois at Chicago, IL 60612 USA.

Publisher Item Identifier S 0278-0062(97)07585-X.



(a)



(b)

Fig. 1. (a) Organization of the range scanner. (b) Schematic diagram of the scanner. When an object is scanned, the point light source, the lens, the mirror, and the camera are fixed. Only the fiber moves over the object. The shadow profile of the fiber on the object is recorded by the camera and used to determine the 3-D coordinates of points on the object.

sizes. Currently, the scanner is set up such that it can scan objects as small as a single tooth and as large as an entire dental cast.

We determine the depths of points on an object through optical triangulation [19]. Fig. 3 shows the optical triangulation principle in both the traditional and the new range scanners. The profile formed on an object is captured by a camera whose orientation is known with respect to the light source. From each image point, the ray from the object that created the image point can be determined. Therefore, assuming the baseline is the line that connects the camera's lens center to the light

source (line AB), by connecting the lens center to a point on the image of a light or a shadow profile, the direction from which the point on the object is viewed (angle α) can be determined. If the baseline length L and the light's direction with respect to the baseline (angle β) are also known, the distance D of the object point to the lens center can then be determined from triangle ABC . Note that the angle between the baseline and the ray connecting the light source to a point on a light or a shadow profile varies slightly with the position of the point. If variation of β along a profile is negligible, then baseline length L and angle of the baseline with the sheet of

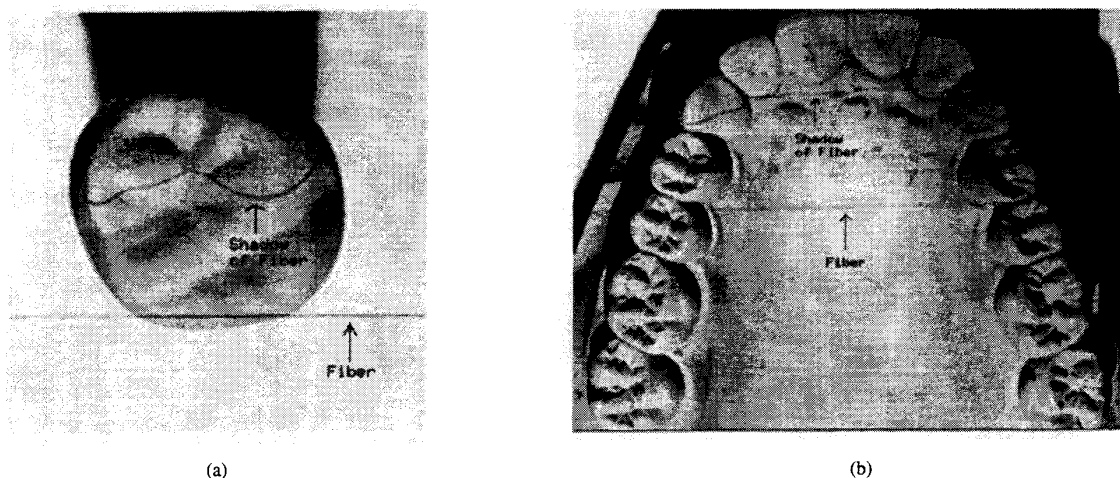


Fig. 2. Examples of images acquired by the camera. The geometry of the shadow profiles are used to determine the coordinates of points on an object.

light β can be determined through a calibration process using a few image points whose 3-D coordinates are known. However, since variation of β along a profile may not be negligible, the coordinates of a large number of image points whose scene coordinates are known are needed to calibrate the scanner.

By rotating the mirror in the implemented scanner, the direction of the cylindrical light changes, which itself changes the baseline length of the scanner. By increasing the baseline length, the accuracy of calculated range values will increase, but it will increase the number of occluded points also. When a very small baseline length is used, an entire shadow profile will be visible from the camera. As the baseline length is increased, more and more points on a shadow profile become hidden from the camera. Therefore, if smooth and convex objects are scanned, a rather large baseline length may be used to achieve highly accurate range values. However, if objects with concavities and sharp edges are scanned, a rather small baseline length should be used to reduce the number of occluded points. Since dental casts contain concavities and sharp edges, in order to reconstruct a cast accurately, the baseline length must be kept large but images from different views of the cast must be obtained and integrated to recover the entire cast.

If the baseline length (L), the angle between the baseline and the optical axis of the camera (α), and the angle between the baseline and the ray connecting the light source to an object point (β) are known, the distance of the object point to the camera (D) can be determined from triangle ABC

$$D = \frac{L \tan \beta}{\cos \alpha (\tan \alpha + \tan \beta)}. \quad (1)$$

If angle β were fixed for all points on a profile, then by determining β and the baseline length L through a calibration process, and by measuring α for each image point, the depths of points in 3-D could be determined from formula (1). However, since angle β varies with points on a profile, and some level of geometric distortion exists in all images due to lens and sensor nonlinearities, we will describe in the following section a calibration method that relates the

coordinates of a large number of points in the scene to the coordinates of their images in the image plane.

Measurement of the depth of a point on a profile requires the ability to locate the image of the profile in the image plane. In our scanner, the light source, the dental cast, and the camera are fixed with respect to each other and only the fiber moves over the cast. If two consecutive image frames are subtracted, all scene intensities will be removed and only intensities corresponding to the difference between the two shadow profiles will remain. Fig. 4(a) and (b) shows two consecutive image frames obtained by scanning a gypsum dental cast, and Fig. 4(c) shows the difference between the two (since negative values cannot be displayed, the absolute values are shown here). If consecutive frames are timed properly, when the frames are subtracted, zero values will be obtained midway between the two profiles, creating a single-pixel-wide zero-crossing contour. The points along a zero-crossing contour as shown in Fig. 4(d) will be used to determine the depths of points in the scene.

Image noise could also result in zero-crossings, but zero-crossings from noise fall randomly in the image, while zero-crossings from subtraction of shifted shadow profiles remain connected. Fig. 4(d) shows the zero-crossings of the difference image after removing noisy zero-crossing contours smaller than eight pixels in length. The threshold length of eight pixels was experimentally found by observing the length of noisy zero-crossing contours in a large number of images.

III. THE CALIBRATION PROCESS

The baseline length (L) and the angle of the baseline with rays connecting the light source to points in the scene (β) must be determined. Since angle β varies from one point to another in the scene, and lens and sensor nonlinearities are present in all cameras at one level or another, a calibration process is needed that takes into account variation in β and image geometric distortions.

To calibrate the scanner, we use the coordinates of a regularly spaced grid points in 3-D and their correspondences

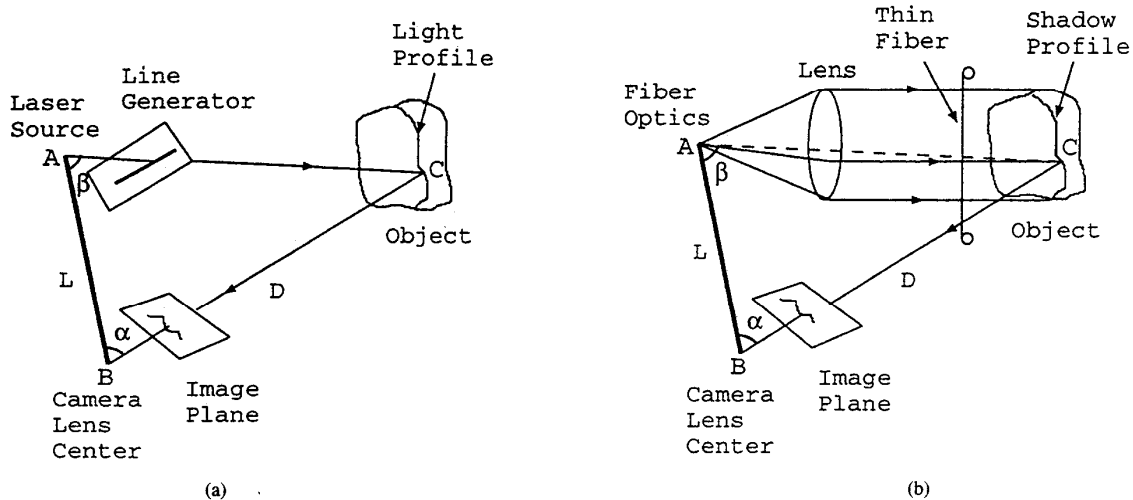


Fig. 3. The optical triangulation principle in (a) the traditional and (b) the proposed range scanners. L is the baseline length and β is the angle between the baseline and the direction of the light. Angle α is obtained by connecting the lens center to an image point on a shadow profile.

in the image plane. To produce a regularly spaced set of 3-D points, we use a translation stage (Melles Griot, Model 07TSZ504) as shown in Fig. 5(a). This translation stage has a $2\text{-}\mu\text{m}$ sensitivity. Lines of $50\text{-}\mu\text{m}$ width and spacing of 0.8 mm are generated on a paper by a 600-dpi postscript printer and the paper is pasted on the stage. The stage is raised to 16 different heights at 0.8-mm intervals. At each height of the stage, the fiber is positioned in 0.8-mm intervals, and at each position of the fiber the stage is scanned. Along each scanline, the intersections of vertical lines on the stage with the zero-crossing contours obtained from the shadow profile are determined. Since the 3-D coordinates of a point corresponding to such an intersection is known from the height of the stage, the horizontal position of the fiber, and the vertical position of the line on the stage, and since the coordinates of the image of the point are known, we can determine the relation between the coordinates of discrete points in the image plane and the coordinates of corresponding points in the scene.

A $51.2 \times 51.2\text{-mm}^2$ area is scanned and quantized into a 64×64 grid at 0.8-mm intervals in x and y directions to obtain a 512×512 image. Also, the translation stage is raised with increments of 0.8 mm at 16 heights to quantize a $51.2 \times 51.2 \times 12.8\text{-mm}^3$ volume into three 3-D arrays of $64 \times 64 \times 16$. The scanning range of 12.8 mm was taken in z direction as opposed to scanning range of 51.2 mm in x and y directions because a volume of $51.2 \times 51.2 \times 12.8\text{ mm}^3$ is sufficient to contain teeth in a dental cast when laid down on a platform. Entry (i, j, k) in the three arrays will show the x , y , and z image values depicted in Fig. 5(b). The point with image coordinates (x, y, z) will, therefore, be at horizontal position $0.8 \times i\text{ mm}$, at vertical position $0.8 \times j$, and at height $0.8 \times k$ in 3-D. In this manner, the obtained tables will relate the coordinates of discrete image points to the corresponding points in 3-D.

Let T_e be the look-up table that relates image coordinates to the elevations of points in the scene. To determine the elevation of a point in 3-D whose image coordinates are

(x, y, z) , we will find table entries that satisfy $Te[i][*][*] \leq x < Te[i+1][*][*]$, $Te[*][j][*] \leq y < Te[*][j+1][*]$, and $Te[*][*][k] \leq z < Te[*][*][k+1]$. The asterisk $*$ means that we may find many table entries satisfying a condition. For instance, $Te[i][*][*]$ means that along the i th column of the array we may find many array entries with different values of j and k that fulfill a condition. Only eight table entries will satisfy all six conditions at any time: $Te[i][j][k]$, $Te[i][j][k+1]$, $Te[i][j+1][k]$, $Te[i][j+1][k+1]$, $Te[i+1][j][k]$, $Te[i+1][j][k+1]$, $Te[i+1][j+1][k]$, $Te[i+1][j+1][k+1]$. These eight entries locate a small cube in 3-D that contains the point whose elevation needs to be determined. We will use the elevations at these eight entries to estimate the elevation at the point by trilinear interpolation. Similarly, the horizontal position and the vertical position of a point in 3-D can be determined from the other two look-up tables.

The 0.8-mm quantization step was selected so that trilinear interpolation would produce an average interpolation error of $60\text{ }\mu\text{m}$. Starting with a quantization step of 4 mm , we determined the difference between actual 3-D coordinates and 3-D coordinates determined by interpolation, and reduced the quantization step until average absolute differences between coordinates of actual and interpolated points were smaller than $60\text{ }\mu\text{m}$. The differences were determined by raising the plate at five random elevations, moving the fiber to five random positions, selecting five random points on a scanline, and determining the absolute difference between the actual horizontal position, vertical position, and elevation of each point and the corresponding values determined by interpolation.

The look-up tables contain information about the baseline length as well as the angles between the baseline length and rays connecting the light source to points in the scene. In addition, the tables contain information about camera distortions. For instance, lens nonlinearity may cause pixels at the center and at the borders of an image to have different sizes, or if the distance between scanlines is not the same as the

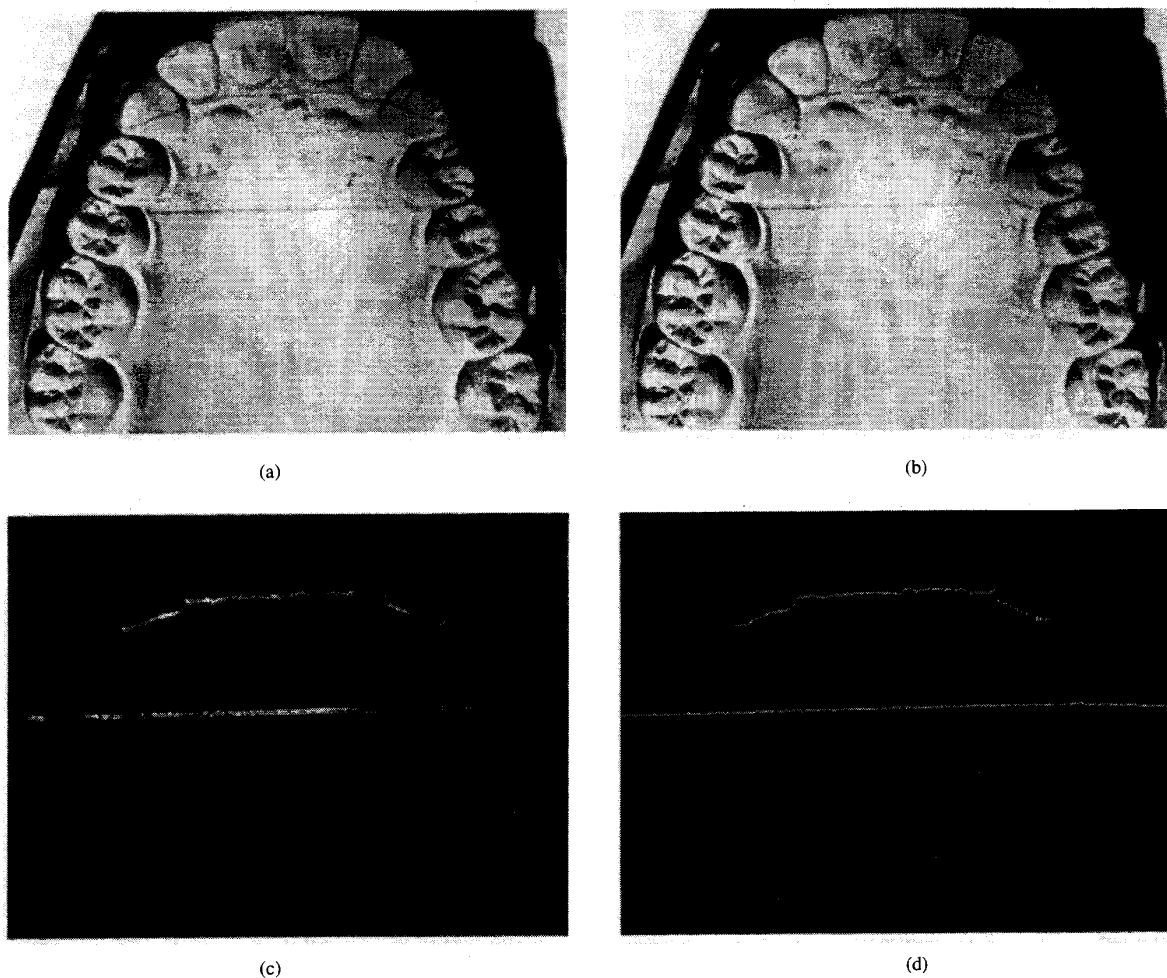


Fig. 4. (a) and (b) Two consecutive image frames from a dental cast. (c) Difference of the two images (only the absolute values are shown here). (d) Zero-crossings of the difference image. The lower profile shows the zero-crossings from the fiber, and the upper profile shows the zero-crossings from the shadow of the fiber.

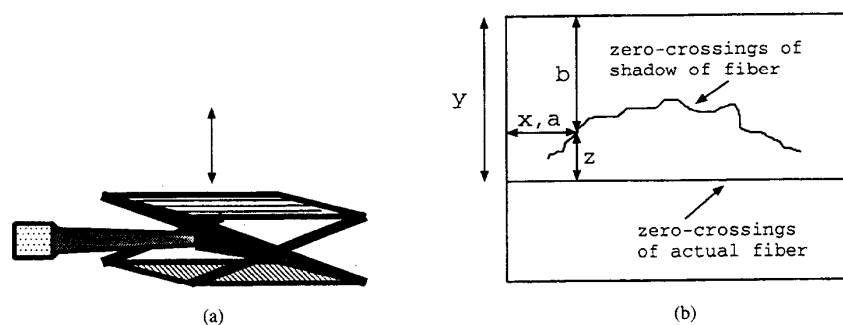


Fig. 5. (a) The translation stage used to calibrate the scanner. (b) Relation between measures x , y , and z and the coordinates (a, b) of an image point. Measures x , y , and z are used to relate the coordinates of points in the image plane to the coordinates of points in 3-D.

distance between pixels in a scanline, image pixels may not be square. Calibrating the camera by preparing the look-up tables in this manner will compensate for image distortions. As long as image distortions remain within a desired tolerance in the discrete steps taken in this calibration process, the tables will be able to compensate for image distortions.

Once the system is calibrated, it can be used as long as the baseline length, the angle between the baseline and the direction of light source, and the camera's zoom and focal length are not changed. If any of these parameters change, the calibration process should be repeated and new look-up tables should be obtained. The calibration process takes about

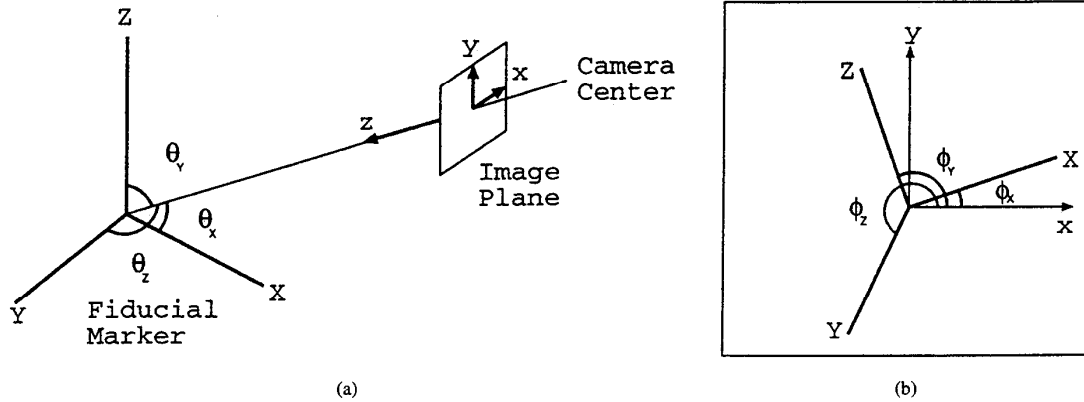


Fig. 6. (a) Relation between the coordinate system of the camera and the coordinate system of the fiducial. (b) Image of the fiducial in the image plane.

20 min, most of which is spent on manually raising the stage and positioning the fiber at equal intervals.

IV. INTEGRATING MULTIVIEW RANGE IMAGES

Traditionally, multiview range images have been integrated by registering them two at a time. To register two images, a transformation function is determined that can map the image in one coordinate system to the image in another coordinate system. Two range images in the same coordinate system are then combined.

Different methods for registering range images have been developed. Gangnon *et al.* [12], Besl and McKey [20], Chen and Medioni [21], and Masuda and Yokoya [23] developed variations of surface matching to register images. These techniques start from an approximate registration and iteratively reach the final registration by minimizing an error functional.

In this paper, we will show that if a special fiducial marker is attached to an object, multiview images of the object can be integrated without image registration. Consider a fiducial marker that is made of three orthogonal axes, and suppose the relation between the fiducial and the camera is as shown in Fig. 6(a). If the fiducial marker is attached to the object during scanning and if we determine the relation between the camera coordinate system and the coordinate system of the fiducial, then images from different views of an object can be transformed into the coordinate system of the fiducial. As a result, the images can be integrated without registering them.

Kanatani [24] has shown that, if an image of three orthogonal axes is given, the orientation of the three axes in 3-D with respect to the optical axis of the camera that obtained the image can be determined. Suppose the coordinate system of the camera is defined in such a way that the optical axis lies on the z -axis and the x - and y -axes, respectively, lie along rows and columns in the image plane. Also, suppose (θ_x, ϕ_x) , (θ_y, ϕ_y) , and (θ_z, ϕ_z) are the spherical coordinates of the X , Y , and Z axes of the fiducial, respectively. Then, it has been shown that [24]

$$\theta_x = \tan^{-1} \sqrt{\frac{-\cos(\phi_y - \phi_z)}{\cos(\phi_x - \phi_y) \cos(\phi_z - \phi_x)}} \quad (2)$$

$$\theta_y = \tan^{-1} \sqrt{\frac{-\cos(\phi_z - \phi_x)}{\cos(\phi_y - \phi_z) \cos(\phi_x - \phi_y)}} \quad (3)$$

$$\theta_z = \tan^{-1} \sqrt{\frac{-\cos(\phi_x - \phi_y)}{\cos(\phi_z - \phi_x) \cos(\phi_y - \phi_z)}} \quad (4)$$

Angles ϕ_x , ϕ_y , and ϕ_z are the angles of the image of the three fiducial axes with the x -axis in the image plane [see Fig. 6(b)].

The fiducial marker may be attached to a dental cast in two different ways, as shown in Fig. 7(a) and (b). In Fig. 7(a), the fiducial is slightly pressed into a dough material in such a way that the axes of the fiducial remain visible from the camera. The dough deforms easily, but if no force is applied to it, its shape remains unchanged. The dough is rather sticky and will stick to the dental cast if slightly pressed against it, as shown in Fig. 7(a). When the dough is secured to a cast, the cast can be moved and the fiducial will move with it.

Another way to secure a fiducial to a dental cast is shown in Fig. 7(b). Here a hook is attached to the fiducial that can grip the bottom of a dental cast. The area beneath the dough and the fiducial marker cannot be imaged. If it is necessary to construct the area underneath the dough, all views of the cast except the top view are obtained with the fiducial intact. Next the dough and the fiducial are gently removed without moving the cast (the cast should be secured in place). The cast is then scanned without changing the position of the camera. Since before the fiducial is removed the orientation of the camera with respect to the cast is known, and since the positions of the cast and the camera have not changed while the fiducial is removed, the orientation of the camera with respect to the cast remains unchanged and known.

Fig. 7(c) shows how a single tooth is secured to a fiducial. The fiducial is first fixated in dough, and then the tooth, which has a hole at the bottom, is inserted into the vertical axis of the fiducial. The dough holding the fiducial and the tooth can now be pressed against a platform and secured in place for imaging purposes. Since one of the axes of the fiducial holds the tooth and is not visible from above, the top view of the tooth should be obtained last. Then the tooth should be gently removed without displacing the fiducial marker in the dough and another image of the fiducial should be obtained. From the

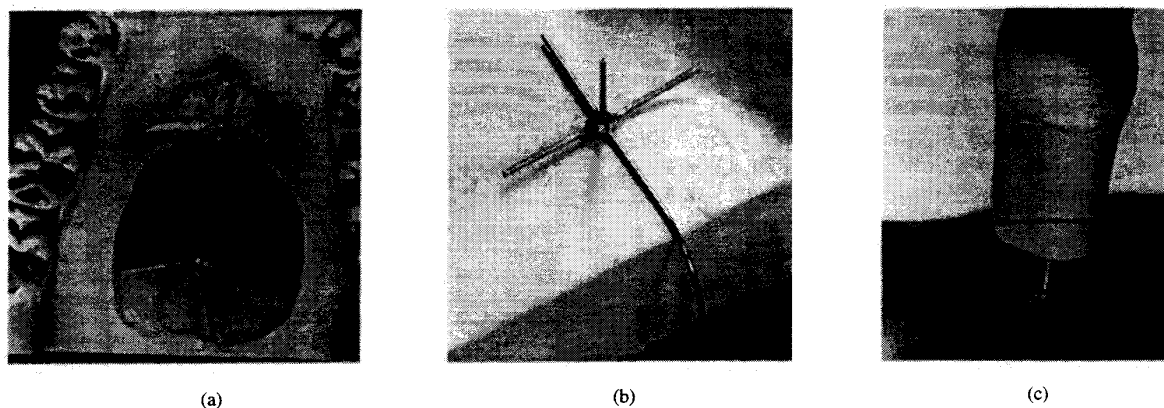


Fig. 7. (a) and (b) Fixating a fiducial marker to a dental cast. (c) Fixating a single tooth to a fiducial marker. When images from different views of a cast or a tooth are obtained with the fiducial marker intact, it becomes possible to integrate the images without registering them.

image of the fiducial without the tooth, the orientation of the camera with respect to the fiducial can be determined. Since the positions of the camera and the fiducial were not changed while removing the tooth from the fiducial, the orientation of the camera with respect to the tooth become known also. In this manner, images from different views of a tooth can be obtained and transformed into the coordinate system of the fiducial and integrated without registering them.

The fiducials shown in Fig. 7(a)–(c) are made of steel wires 0.6 mm in diameter and 8 mm in length. The function of a fiducial is to enable transformation of range values obtained in the viewer-centered coordinate system to range values in the coordinate system defined by the fiducial. In this manner, images obtained from different views of a dental cast or a tooth are transformed to images in the same coordinate system and integrated without image registration.

V. RESOLUTION AND ACCURACY OF THE SCANNER

Resolution along a scanline (x direction) is determined from the number of samples taken on the scanline. When the frame grabber digitizes a scanline into 512 samples and the scanline covers a length of 51.2 mm in the scene, the resolution of the scanner along the scanline will be $51.2/512$ mm, or $100 \mu\text{m}$. Resolution between scanlines (y direction) is determined from the distance the fiber travels in the scene while obtaining two consecutive scanlines. When a 51.2-mm length is scanned 512 times in equal intervals, the resolution of the scanner in y direction will be $51.2/512$ mm, or $100 \mu\text{m}$.

We have adjusted the scanner so that profiles of widths from one to three pixels are obtained in the image plane, and we have adjusted the speed of the translation stage so that it travels a distance of $100 \mu\text{m}$ between two consecutive frames. If the distance between consecutive scans is too large, zero-crossing contours will not be obtained. If the distance traveled is too small, the shadow profiles will fall on top of each other, again making detection of the zero-crossing contours impossible.

To determine the resolution in the z direction, we use the translation stage shown in Fig. 5(a). Suppose the vertical distance of a zero-crossing corresponding to a point on the stage to the zero-crossing corresponding to the fiber is z_1

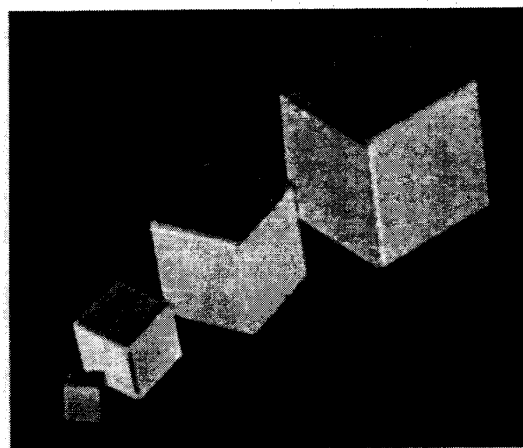


Fig. 8. Four cubes with sides measuring 10, 20, 30, and 40 mm were used to determine the accuracy of the scanner.

pixels. We raise the stage d mm and again determine the distance of the obtained zero-crossing to the zero-crossing of the fiber. Suppose the obtained distance is z_2 pixels. The resolution of the scanner in the z direction will, therefore, be $d/(z_2 - z_1)$ mm. In our scanner we raised the stage by 2 mm to obtain $(z_2 - z_1)$ equal to 20 pixels. Therefore, resolution in z direction was $2/20$ mm, or $100 \mu\text{m}$.

In our scanner, we use a strand of human hair as the fiber to generate the shadow profiles. The hair diameter in our experiments has been about $50 \mu\text{m}$. The system grabs 30 frames/s, the motor that controls the translation stage rotates three revolutions per second, and each revolution translates the hair by 1 mm. Therefore, the distance between consecutive scanlines is $100 \mu\text{m}$. When the camera digitizes a 51.2×51.2 -mm² area into a 512×512 -pixel image, the resolution along the scanline will be $100 \mu\text{m}$. The angle of the mirror is set in such a way that if the platform is raised by 1 mm, its profile in the image plane will shift by ten pixels, thereby producing a resolution of $100 \mu\text{m}$ in the direction normal to the platform.

To determine the calibration accuracy, we used the translation stage shown in Fig. 5(a). We set the elevation of the

stage at ten random heights, and at each height moved the fiber to ten random positions, and on each obtained profile, selected ten random points. This gave us 1000 random points in 3-D whose coordinates were known. We then determined the elevations of the points from the calibration table, using trilinear interpolation as discussed in Section III. Computed elevations were then subtracted from the actual ones. Absolute differences were determined and their mean and maximum were found to be $62 \mu\text{m}$ and $300 \mu\text{m}$, respectively. Standard deviation of the absolute differences was $28 \mu\text{m}$. This shows that more than 90% of the measurements obtained by the scanner were within $100 \mu\text{m}$ of the actual values.

To determine the accuracy of the image integration process, four cubes with sides measuring 10 mm, 20 mm, 30 mm, and 40 mm, as shown in Fig. 8, were prepared by our instrument shop and polished to a surface accuracy of $30 \mu\text{m}$. Since three edges of a cube that meet at a corner form a coordinate system, we used a corner and the edges that formed it as the fiducial. Images from the top and four sides of the cubes were obtained and the images were integrated according to the procedure outlined in Section IV.

When obtaining the images, we made sure that three edges of a cube that formed a corner were visible in each image. The three edges were then used as our fiducial. Since the geometry and size of each cube were known, the relation between the coordinate system centered at one cube corner and the coordinate system centered at another cube corner could be determined. Range images were manually segmented to extract the sides of the cube. Planes were fitted to range values from the top and four sides of each cube, and the intersections of the planes were used as the cube edges and corners. Maximum and average distances between the planes representing the sides of the cubes and the range values that determined them were computed and entered into Table I. The distances, which are referred to by errors in the table, are in μm . Average and maximum errors in computation of the lengths of the sides of each cube were also determined and entered into Table I. In addition, average and maximum errors of 20 visible angles between adjacent edges of each cube were determined and entered into Table I. Here, the numbers are shown in mrad. All measurements were obtained under the same calibration parameters. Some of the errors were as large as $300 \mu\text{m}$ due to image noise, but more than 90% of the range values had errors less than $100 \mu\text{m}$, with a mean of $50 \mu\text{m}$ for the faces and a mean of $75 \mu\text{m}$ for the edges of the cube.

VI. RESULTS

To show examples of range images obtained by this scanner, an ivory tooth, as shown in Fig. 9(a) and (b), was used. This model tooth is not completely opaque, so it transmits some of the light reaching it, making the shadow profiles not clearly visible. To make the surface of the tooth more opaque and also to reduce its specularity, the tooth was sprayed with a matte material, as shown in these images. Scanning the top and the four sides of the tooth with our scanner, we obtained the range images shown in Fig. 9(c)–(g). Brighter points show higher elevations in these images. The images were integrated according to the procedure described

TABLE I
IMAGE INTEGRATION ACCURACY. ERRORS IN RECOVERY OF THE FACES
AND EDGES OF THE CUBES ARE IN μm . ERRORS IN RECOVERY
OF THE ANGLES BETWEEN THE EDGES OF THE CUBES ARE IN mrad

	10-mm cube	20-mm cube	30-mm cube	40-mm cube
Max. Error of faces	260	280	300	290
Mean error of faces	48	44	43	52
Max. error of edges	310	320	290	330
Mean error of edges	78	72	80	74
Max. error of angles	4.5	3.3	3.0	3.2
Mean error of angles	1.5	1.3	1.2	0.

in Section IV, obtaining Image 9(h). There are a few small holes in the obtained range image due to missing data. To recover data corresponding to these holes, further images that cover the areas must be obtained. Missing data in these small areas can also be recovered by fitting a smooth surface to the data. The surface-fitting process will not only recover missing data, but also make graphical rendering of the tooth possible. Fitting a rational Gaussian surface [25] to the data of Fig. 9(h), we obtain the surface shown in Fig. 9(i) and (j). Comparing images 9(i) and 9(j) with images 9(a) and 9(b), respectively, we see that the geometry of the tooth has been recovered. The surface-fitting process fills in the missing data, but it smooths the data. If measurements on a tooth are required, one must use range Image 9(h). The surface-fitting process will smooth out sharp tooth details and is primarily for visualization purposes. To achieve more details in a reconstructed tooth one may use a more elastic surface. A very elastic surface, however, will retain noisy surface details that may not be desirable. One may interactively vary the elasticity of the surface and choose the right elasticity, observing the reconstructed surface.

An example of a mandibular dental cast is shown in Fig. 10. Fig. 10(a) shows the original dental cast, while Fig. 10(b)–(e) shows four scans of the cast from slightly different views from above the cast. Due to sharp concavities in the cast, occluded points are obtained in some of the views (as shown by holes in the images). Multiple-view images are necessary to cover all the concavities. After the four images are integrated, the cast was reconstructed in 3-D, as shown in Fig. 10(f)–(h). The images show the raw range values without elastic surfaces fitted to them. Since only information from the top of the cast is obtained in the range images shown in Fig. 10(b)–(e), the program that renders a reconstructed cast automatically fills in missing data on the sides of the cast with vertical lines.

Our scanner is controlled by a Sun Sparc V. Since this computer is not fast enough to process the images as they are acquired, the images are saved first and processed later. It takes 20 s to scan one view of a dental cast and about 3 min to process them and determine the range images. Combining multiview range images takes another 3 min. The entire process, therefore, requires about 20 min to scan and reconstruct a dental cast.

The range images are acquired automatically. However, to integrate multiple-view images, the fiducial axes in one of the images must be determined interactively. This interaction involves selecting with the mouse a point on each axis of the

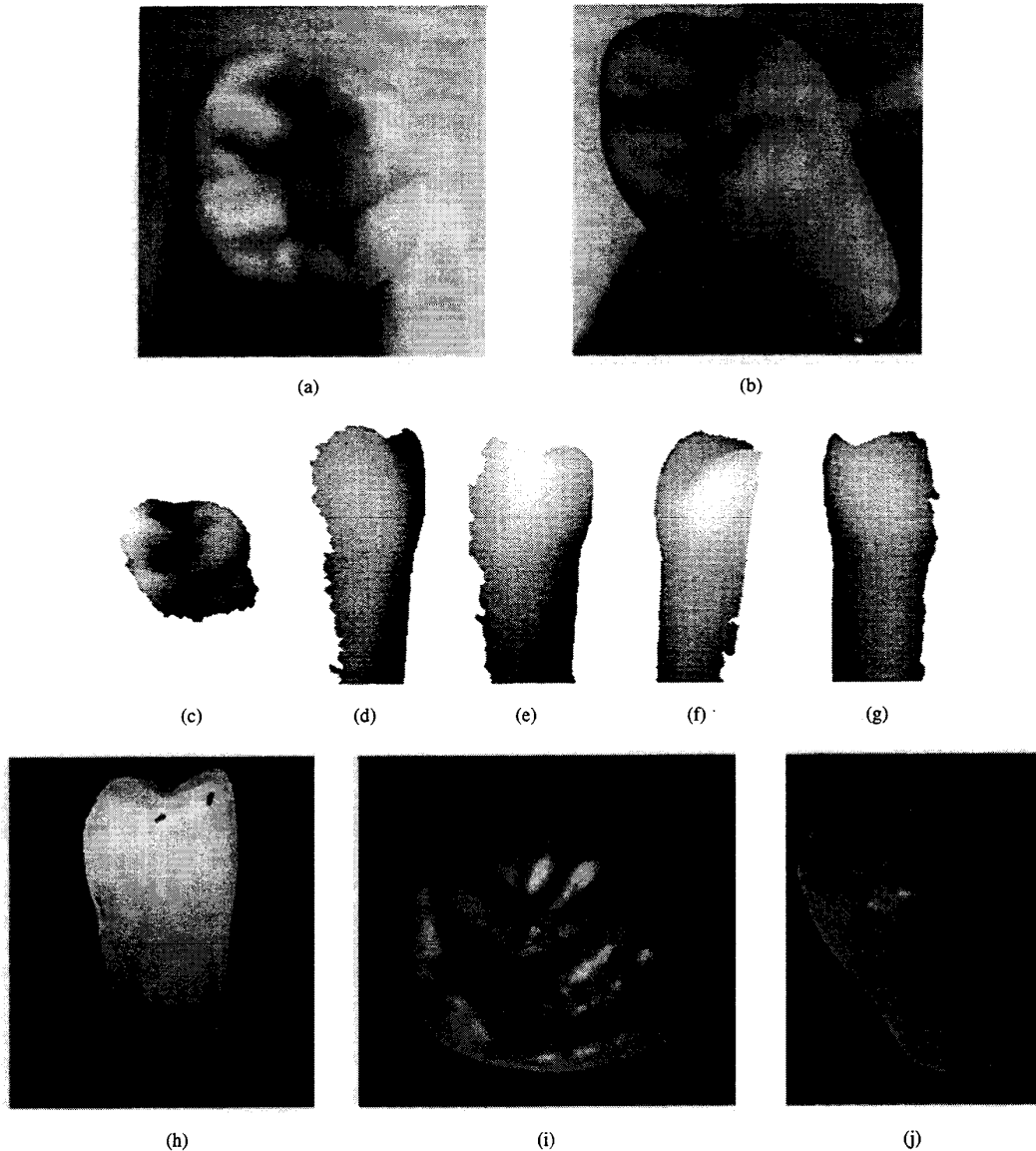


Fig. 9. (a) and (b) Two different views of a model tooth. (c)–(g) Range images from the top and four sides of the tooth. (h) Digital tooth obtained by combining range Images (c)–(g). (i) and (j) Two different views of the reconstructed tooth.

fiducial and the point where the three axes join in the image plane. This interaction usually takes about 1 min. To make the system totally automatic, an algorithm that automatically detects the fiducial axes should be developed. Although the current system requires about 20 min to scan and construct a dental cast, only a few minutes of that require user supervision. The rest of the time, which involves pure computation, can be carried out in the background without user interaction.

VII. CONCLUSIONS

Digital reconstruction of gypsum dental casts has tremendous applications. A digital dental cast can be saved along with patient data and retrieved conveniently when necessary. It can be transmitted over the network for remote diagnosis by a dentist. It can be used to measure distances and orientations of

teeth with respect to each other. It also can be used to design restorations. This paper has described the details of a range scanner that can transform a gypsum dental cast into a digital model for storage and display purposes. The scanner is based on white light and uses the subtractive light principle to create very thin shadow profiles on a dental cast. When scanning a $51.2 \times 51.2\text{-mm}^2$ dental cast into a 512×512 image, we obtain a theoretical resolution of $100 \mu\text{m}$. The average and standard deviation errors in determining elevations of points in dental casts were $62 \mu\text{m}$ and $28 \mu\text{m}$, respectively, and the average and standard deviation errors in integrating multiview images were $80 \mu\text{m}$ and $36 \mu\text{m}$, respectively.

Image integration is achieved by attaching a special fiducial marker to the object before scanning. The fiducial marker is used to define a local coordinate system for the object

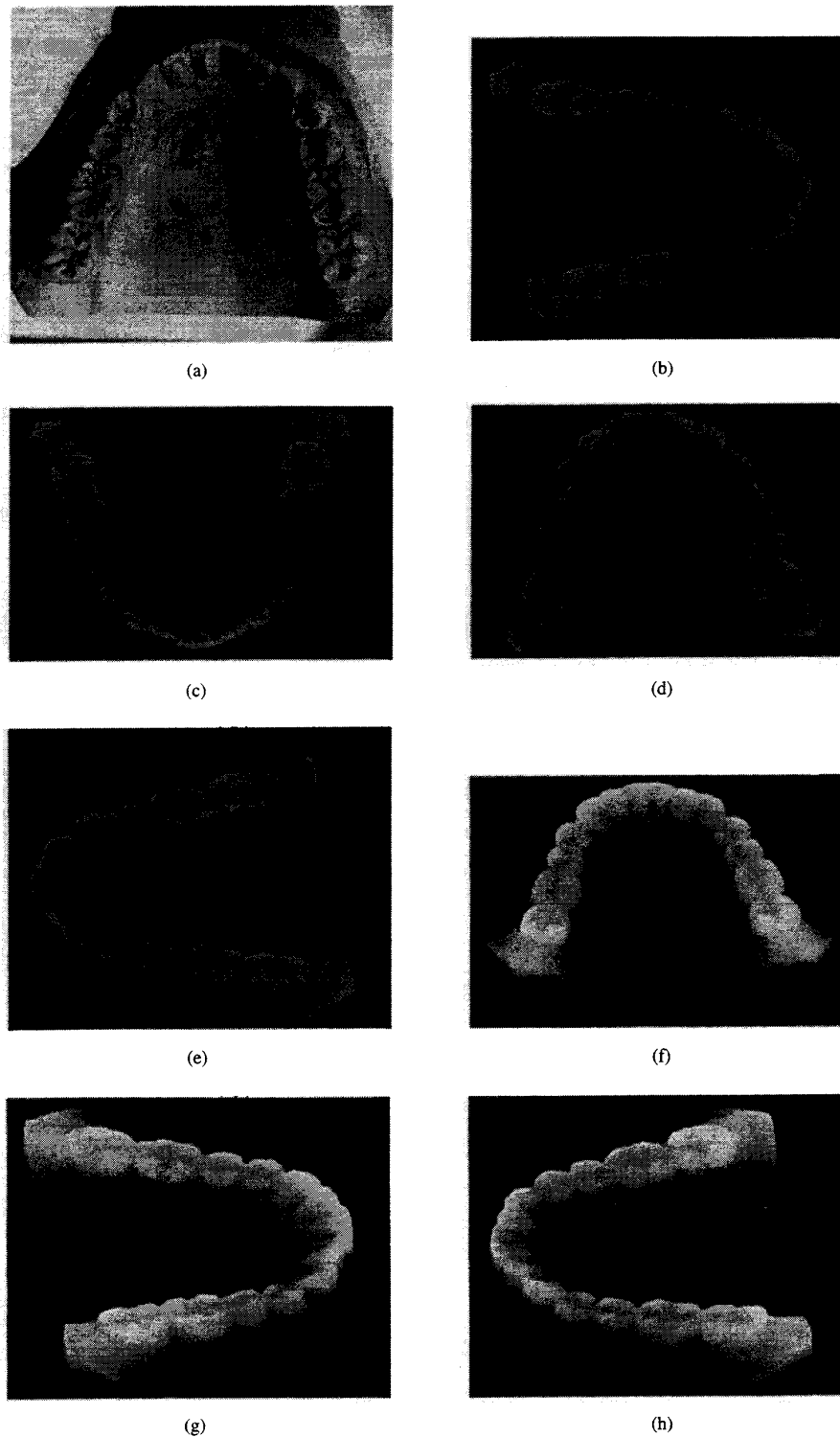


Fig. 10. (a) A mandibular dental cast. (b)–(e) Four scans of the cast obtained from slightly different view directions. (f)–(h) The reconstructed cast shown in three different views.

so that data from different views can be resampled to the same coordinate system. Use of the proposed fiducial marker makes it possible to integrate multiview range images of a cast without registering them.

The scanner as described in this paper can be further improved. A method to automatically detect the fiducial axes in the images is desirable and will remove the need for user interaction. A higher resolution frame grabber and camera will

increase the resolution of obtained images and increase the accuracy of the measurements. A faster computer will enable processing of the images as they are captured rather than scanning them first and processing them later.

REFERENCES

- [1] S. Berkowitz and S. Pruzansky, "Stereophotogrammetry of serial casts of cleft palate," *Angel Orthod.*, vol. 38, pp. 136-149, 1968.
- [2] S. Berkowitz, "Stereophotogrammetric analysis of casts of normal and abnormal palates," *Amer. J. Orthod.*, vol. 60, pp. 1-18, 1971.
- [3] S. Berkowitz, G. Gonzalez, and L. Nghiem-Phu, "An optical profilometer—A new instrument for the three-dimensional measurement of cleft palate casts," *Cleft Palate J.*, vol. 19, pp. 129-138, 1982.
- [4] B. S. Savara, "Applications of photogrammetry for quantitative study of tooth and face morphology," *Amer. J. Phys. Anthropol.*, vol. 23, pp. 427-434, 1965.
- [5] F. P. G. M. van der Linden, H. Boesma, T. Zelders, K. A. Peters, and J. H. Raben, "Three-dimensional analysis of dental casts by means of the Optocom," *J. Dent. Res.*, vol. 51, p. 1100, 1972.
- [6] G. W. Butcher and C. D. Stephens, "The reflex optical plotter—A preliminary report," *Br. Dent. J.*, vol. 151, pp. 304-305, 1981.
- [7] K. Tanaka, A. A. Lowe, and R. DeCou, "Operational performance of the Reflex Monograph and its applicability to the three-dimensional analysis of dental casts," *Amer. J. Orthod.*, vol. 83, pp. 195-199, 1983.
- [8] S. N. Bhatia and V. E. Harrison, "Operational performance of the traveling microscope in the measurement of dental casts," *Br. J. Orthod.*, vol. 14, pp. 147-153, 1987.
- [9] F. Livingstone, "Application of laser digitizing to automotive design and inspection," *Body Eng. Design, Development*, vol. 17, no. 2, pp. 1-4, 1989.
- [10] M. Rioux, J. A. Beraldin, M. O'Sullivan, and L. Courmoyer, "Eye-safe laser scanner for range imaging," *Appl. Optics*, vol. 30, no. 16, pp. 2219-2223, 1991.
- [11] M. Rioux, "Color 3-D electronic imaging of the surface of the human body," in *Proc. Society of Photo-Optical Instrumentation Engineers*, San Diego, CA, July 28-29 1994, vol. 2277, pp. 42-54.
- [12] K. Yamamoto, A. Toshimitsu, T. Mikami, S. Hayashi, R. Harada, and S. Nakamura, "Optical measurement of dental cast profile and application to analysis of three-dimensional tooth movement in orthodontics," *Frontiers Med. Biol. Eng.*, vol. 1, pp. 119-130, 1988.
- [13] K. Yamamoto, S. Hayashi, H. Nishikawa, S. Nakamura, and T. Mikami, "Measurements of dental cast profile and three-dimensional tooth movement during orthodontic treatment," *IEEE Trans. Med. Imag.*, vol. 38, no. 4, pp. 360-365, 1991.
- [14] F. Duret, J.-L. Blouin, and B. Duret, "CAD-CAM in dentistry," *J. Amer. Dent. Assoc.*, vol. 117, pp. 715-720, Nov. 1988.
- [15] H. O. Heymann, "CAD/CAM for ceramic inlays and onlays: The CEREC system," in *Trans. Acad. Dent. Mat., Proc. Conf. CAD/CAM in Dentistry*, Feb. 17, 1989, vol. 2, no. 1, pp. 8-16.
- [16] M. Brandestini and W. Mörmann, *Computerized Processing of Ceramic Fillings in the Dental Operatory*. Bensheim, Germany: Siemens AG, Dental Sector, 1988.
- [17] E. D. Rekow, "CAD/CAM for crowns," in *Trans. Acad. Dent. Mat., Proc. Conf. CAD/CAM in Dentistry*, Feb. 17, 1989, vol. 2, no. 1, pp. 17-20.
- [18] ———, "A review of the developments in dental CAD/CAM systems," *Prosthodontics and Endodontics*, S. D. Campbell, M. Siskin, Sr., and H. Martin, Eds., 1992, pp. 25-33.
- [19] R. Jain, R. Kasturi, and B. G. Schunck, *Machine Vision*. New York: McGraw-Hill, 1995, pp. 359-360.
- [20] P. J. Besl and N. D. McKay, "A method for registration of 3-D shapes," *IEEE Trans. Pattern Anal. Machine Intell.*, vol. 14, pp. 239-256, 1992.
- [21] Y. Chen and G. Medioni, "Object modeling by registration of multiple range images," *Image and Vision Computing*, vol. 10, no. 3, pp. 145-155, 1992.
- [22] H. Gangnon, M. Soucy, R. Bergevin, and D. Laurendeau, "Registration of multiple range views for automatic 3-D model building," in *Proc. 1994 IEEE Conf. Computer Vision and Pattern Recognition*, Seattle, WA, June 21-23, 1994, pp. 581-586.
- [23] T. Masuda and N. Yokoya, "A robust method for registration and segmentation of multiple range images," *Comput. Vision, Image Understanding*, vol. 61, no. 3, pp. 295-307, 1995.
- [24] K. Kanatani, "The constraints on images of rectangular polyhedra," *IEEE Trans. Pattern Anal. Machine Intell.*, vol. PAMI-8, no. 4, pp. 456-463, 1986.
- [25] A. Goshtasby, "Geometric modeling using rational Gaussian curves and surfaces," *Comput. Aided Design*, vol. 27, no. 5, pp. 363-375, 1995.